INDIAN JOURNAL OF SCIENCE AND TECHNOLOGY

Check for updates

* **Corresponding author**.

pratimasardar07@gmail.com

Simultaneous removal of lead and cadmium ions by nickel oxide nanoparticles

Pratima Rani Sardar[1]*

1 Department of Botany, Sivaji College, University of Delhi, New Delhi, 110027

Abstract

Objectives: To study the simultaneous removal of metal ions to understand the dynamics of the adsorption process for the assessment of the actual potential of an adsorbent in real-life applications. **Methods:** A one-step hydrothermal method was employed for the synthesis of nanomaterial. The hydrothermal treatment was performed at 110°C for 3 hours and calcined at 300°C for 2 hr to complete the nickel oxide nanoparticle synthesis. A systematic study of metal ion adsorption onto the nickel oxide nanoparticle was conducted to evaluate the maximum adsorption capacity and to understand the adsorption behaviour of the metal ions in presence of the others. The estimation of metal ion adsorption was done by measuring the residual concentrations using an atomic absorption spectrophotometer. **Findings:** The microscopic and spectroscopic characterizations confirmed the formation of nickel oxide nanostructures. The experimental results suggested that the adsorption process follows the Langmuir isotherm and the pseudo-second-order model for metal ion adsorption in single and mixed solutions. A synergistic effect was observed for Pb (II) adsorption and an antagonistic effect for Cd (II) adsorption. The maximum adsorption capacity of ~650 mg/g of Pb (II) and ~475 mg/g of Cd (II) were noticed for simultaneous adsorption by the NiO nanoparticle. **Novelty/improvement:** The presence of more than one heavy metal ion in the wastewater is obvious, and one kind of metal ion may interface with the adsorption behaviour of the others. Further, limited studies on simultaneous adsorption of metal ions using metal-oxide nanoparticles are available in the literature. Hence, this work will provide an idea about the applicability of the NiO nanoparticle for real-life applications.

Keywords: Adsorption; NiO; Heavy metal ions; Simultaneous removal

1 Introduction

Transition metals and metal oxides have been receiving significant attention because of their diverse applications in the field of catalysis[1,2], batteries[3], electromagnetism[4], gas sensors[5,6], and photocatalysis[7,8]. These metal/metal oxide-based nanomaterials possess a large surface-to-volume ratio, unique adsorptive properties, surface defects,

and fast diffusivities[9,10]. These materials are of much interest because of their unique shape and size-dependent properties[11,12] as compared to bulk crystals with the same chemical composition. At the nanoscale level, the size and shape of particles play an important role in determining the optical, magnetic, and electronic properties of the materials.

In recent time, Nickel oxide (NiO) have gained much attention in various applications such as catalysis, energy, and environmental remediation due to its superior chemical, magnetic, and optical properties, and thermal stability[13–15]. The ease of synthesis and possibilities to making a very high surface mesoporous structure make the NiO a potential adsorbent for the removal of metal ions[15]. There are reports on the efficient removal of toxic metal ions using various NiO and NiO-based hybrids[16–18]. Most of the research reported the performance evaluation of the nanomaterial as an adsorbent in the presence of single ion solutions. However, very limited studies can be seen in the literature related to the adsorption performance in the presence of binary or multiple ion solutions.

Generally, wastewater contains various kinds of pollutants such as organic pollutants and inorganic pollutants[19,20]. Among the inorganic pollutants, the presence of one or more heavy metal ions in wastewater is common in most cases. Furthermore, the presence of one metal ion can interfere with the adsorption behavior of other metal ions and may alter the removal efficiency as well as adsorption kinetics[18]. Hence, it is imperative to evaluate the adsorption performance of an adsorbent in presence of multiple metal ions to assess the potential for real-life applications.

Here, I report, the evaluation of the nanomaterial's potential for metal ion removal and their adsorption characteristics in a multicomponent system. A hydrothermal route was followed for the synthesis of the nanoparticle. Adsorption studies were conducted in the presence of single metal ions and binary metal ions. The experiments were designed in a unique combination of the parameter to get a clear idea about the adsorption pattern in a single as well as in a binary metal ion-containing system. The equilibrium studies provide an idea about the adsorption capacity of the nanomaterial and the kinetics experiments provide an insight into the factors that affect the adsorption process. Various microscopic and spectroscopic characterizations were performed to confirm the NiO formation.

Cadmium and lead ions are the two common metal ions that are available in most of the wastewater. These metal ions are toxic and are responsible for many health-related issues. Long-time exposure to these metal ions may affect human health and can be the reason for cancer too[20,21]. Hence, Cd (II) and Pb (II) were selected for the experiments. Adsorption studies suggested a synergistic effect for Pb (II)adsorption and an antagonistic phenomenon for Cd (II)adsorption for simultaneous removal of ions.

2 Materials and Methods

Analytical grade nickel chloride (NiCl$_2$.6H$_2$O), sodium hydroxide (NaOH), ammonia solution (NH$_3$.H$_2$O), cadmium nitrate [Cd (NO$_3$)$_2$], and lead nitrate [Pb (NO$_3$)$_2$] ethanol from Sigma Chemicals were used without any further purification for the experiments.

2.1 NiO nanostructure synthesis

A hydrothermal method was employed to synthesize NiO nanoparticles. 0.1 M precursor solution was prepared by dissolving the nickel salt in deionized (DI) water. The pH of the solution was adjusted to 9 using 0.01M NaOH solution. The NH$_3$H$_2$O solution was then added to the solution and transferred into a Teflon-coated autoclave. Further, the autoclave was kept inside a furnace at 110 °C for 3 h to complete the reaction. Finally, the reaction solutions were taken out from the autoclave, washed with DI water after cooling down, and heated at 300 °C in presence of oxygen for 2 h to complete the NiO nanoparticle formation.

2.2 Characterizations

Field emission scanning electron microscopy (FESEM) (FEI Quanta 200) was used to see the morphology of the nanoparticles. The elemental analysis was done by capturing the energy-dispersive X-ray spectra (EDS) using an Oxford-EDX system. The X-ray diffraction of the NiO nanoparticles was done for phase identification of crystalline material using CuK$_\alpha$ radiation (λ = 0.15418 nm) (Netherland PANalytical X'Pert PRO diffractometer).

2.3 Adsorption Study

All experiments were performed in batches mode. 0.1 mg of nanomaterial was used as an adsorbent for every mL of solution for all experiments. A stock solution was used as a source for getting the solutions of various concentrations. The serial-dilution technique was employed to get those diluted solutions. The stock solutions of 500 mg/L of Cd (II) and Pb (II) were prepared by dissolving the respective salt in DI water. After completion of each experiment, the solution was centrifuged to separate the

solid adsorbent, and the residual metal ion concentration was estimated using an atomic absorption spectrophotometer (AAS). Initial heavy metal ion concentrations of 5 mg/L to 300 mg/L range were taken for the adsorption equilibrium studies and a fixed concentration of 100 mg/L was used for kinetic studies.

The adsorption capacity was computed using **Equation 1**.

$$Adsorption\ capacity\ (q_e) = \frac{(C_0 - C_e)V}{m} \tag{1}$$

In Equation 1, C_0 and C_e are the initial and equilibrium metal ion concentrations in mg/L, V is the solution volume in mL, and m is the amount of nanomaterial in mg.

Kinetic experimental data were fitted using two known model equations: pseudo-first-order **(Equation 2)** and pseudo-second-order **(Equation 3)** to find the progression of the adsorption process with time[17,22].

$$log\ (q_e - q_t) = log\ q_e - \frac{k_1 t}{2.303} \tag{2}$$

$$\frac{t}{q_t} = \frac{1}{k_2 q_e^2} + \frac{t}{q_e} \tag{3}$$

In the Equation 3, q_t (mg/g) and q_e (mg/g) are the amounts of ion adsorbed at time t (min) and equilibrium, respectively; k_1 (min^{-1}) and k_2 (g.mg^{-1}.min^{-1}) are the rate constant of the respective rate equations.

Equilibrium experiments were conducted to estimate the adsorption capacity of the nanomaterial. Two commonly used isotherms, the Langmuir isotherm which is given in **Equation 4** [22], and the Freundlich isotherm which is given in **Equation 5**[22] were used for experimental data analysis.

$$\frac{C_e}{q_e} = \frac{1}{bq_{max}} + \frac{C_e}{q_{max}} \tag{4}$$

Where q_{max} (mg/g) is the maximum adsorption capacity. b (L/g) is the Langmuir adsorption constant.

$$logq_e = logk_f + \left(\frac{1}{n}\right) logC_e \tag{5}$$

Where k_f (mg.g^{-1}.L$^{1/n}$.mg$^{-1/n}$ and n (dimensionless) are the Freundlich adsorption constants and adsorption coefficient, respectively.

The separation factor (R_L) is a dimensionless parameter. It can be calculated by using **Equation 6**.

$$R_L = \frac{1}{1 + bC_0} \tag{6}$$

R_L provides information regarding the process's feasibility. If the R_L value of a process is < 1, then the process is considered to be favorable[17].

3 Results and Discussion

3.1 Characterization of NiO nanostructures

The morphology of the nanostructures was captured using a FESEM. The FESEM image of the nanomaterial is presented in Figure 1**a**. An aggregated structure of globular NiO particles is evident in the SEM image. The development of pore generation in the nanostructure is also visible from the FESEM image. The presence of nickel and elemental oxygen was confirmed from the EDS spectrum analysis of the nanomaterial (Figure 1**b**).

The crystallinity of the nanostructures was done by using X-ray diffraction (XRD). The XRD pattern of the nanostructures is shown in Figure 1**c**. The characteristic peaks at 2q = 37.26°, 43.29°, 62.89°, 75.43°, 79.43° are assigned to (111), (200), (220), (311) and (222) planes corresponds to NiO cubic structure (JCPDS no- 78-0643)[23].
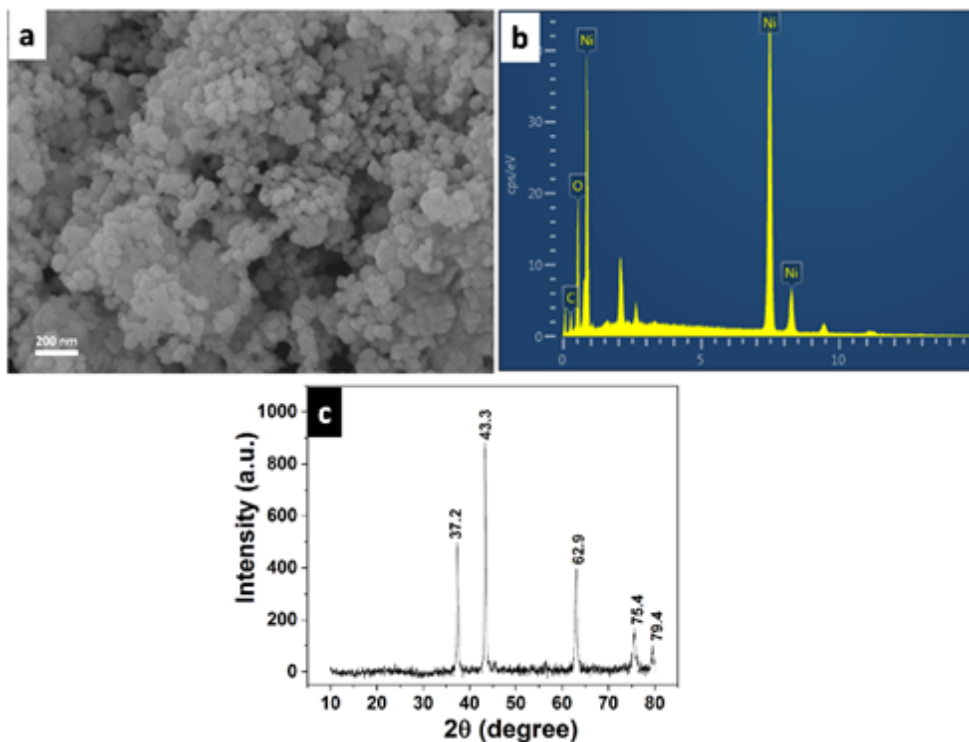
Fig 1. (a)FESEM image, (b) EDS spectrum, and (c) XRD of NiO nanoparticles

3.2 Adsorption Studies in the presence of single ions

For the equilibrium experiments, 5 mg/L to 300 mg/L concentrations of Cd (II) and Pb (II) were taken.Figure 2a shows the equilibrium adsorption capacities of NiO as a function of equilibrium concentrations of the respective metal ions. An exponential decay kind of plot was found for both types of metal ions where the curves follow a sharp increase in adsorption capacity, further plateaued to a fixed value of adsorption capacity with increasing metal ion concentrations. The q_{max} of the nanomaterial was to found be ~610 and ~515 mg./g for Cd (II) and Pb (II), respectively.

The experimental results after analyzing plotted in terms of Langmuir and Freundlich isotherm in Figure 2b and Figure 2 c, respectively. The values of the constants corresponding to the respective model equations were computed from the C_e/q_e versus C_e plot and $logq_e$ versus $logC_e$ plot, respectively, and presented in Table 1. The correlation coefficient (R^2) value of the model fitting equations was found to be higher for Langmuir isotherm compared to the Freundlich isotherm indicating that the Langmuir isotherm can better explain the metal ion adsorption on NiO nanoparticles data. Further, a positive and <1 values of R_L for all cases [R_L = 0.114 – 0.939 for Cd (II) and R_L = 0.057 – 0.866 for Pb (II)] confirmed the favorable adsorption of metals ions onto NiO.

Table 1. The parameters of Langmuir and Freundlich isotherm for Cd (II) and Pb (II) adsorption onto NiO nanostructures.

	Single-component		Binary-component	
	Cd (II)	Pb (II)	Cd (II)	Pb (II)
Langmuir				
q_{max} (mg/g)	~515	610	~475	~650
b (L/mg)	0.01	0.02	0.01	0.02
R^2	0.99	0.99	0.98	0.99
Freundlich				
k_f ((mg.g^{-1})(L$^{1/n}$.mg$^{-1/n}$))	15.40	21.20	14.30	22.76
n	1.37	1.58	1.59	1.67
R^2	0.96	0.96	0.951	0.967
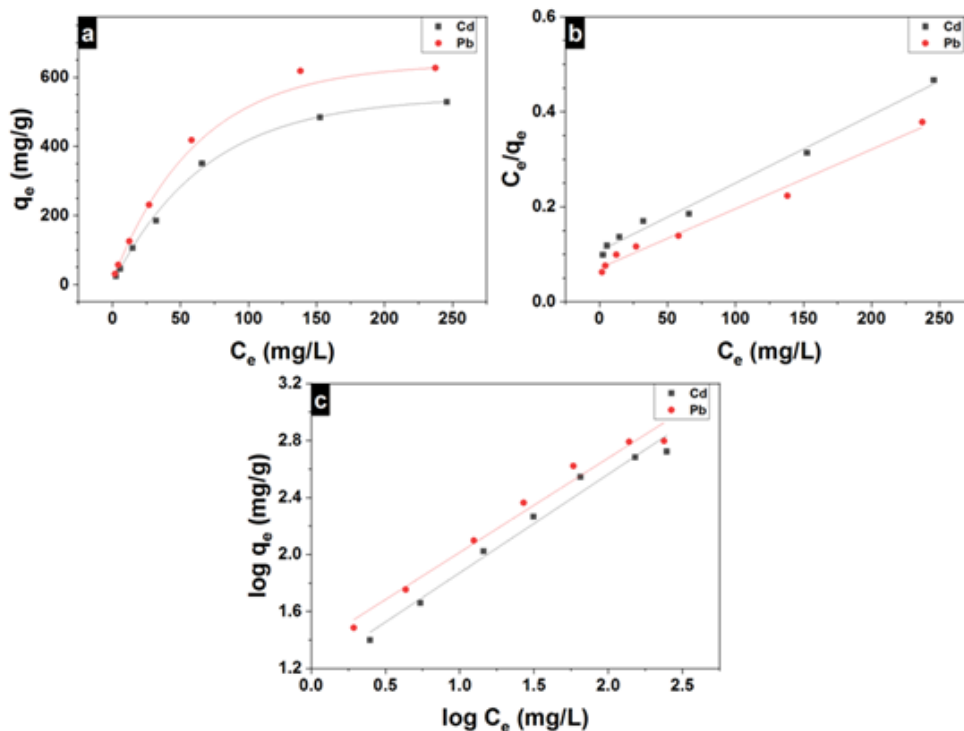
Fig 2. (a) q_e versus C_e plot, (b) Langmuir isotherm, (c) Freundlich isotherm for Cd (II) and Pb (II) adsorption NiO.

Figure 3a represents the time-dependent adsorption capacity of the nanomaterial. It has been noticed that the adsorption capacity is increasing with the increase in adsorption time. However, no significant change in adsorption capacity was observed after 60 min of the experiment. The experiment data were fitted using both the proposed model equations and presented in Figure 3**b** and Figure 3**c**, respectively. The model parameters of the respective equations were also calculated and presented in Table 2. The pseudo-second-order model fitting provides a higher correlation coefficient (R^2) compared to the pseudo-first-order model fitting. These findings indicated that the time-dependent metal ion adsorption process could be better explained by a pseudo-second-order kinetic model equation.

Table 2. The parameters of the model kinetic equations for Cd (II) and Pb (II) adsorption onto NiO.

	Single component		Binary component	
	Cd (II) [100 mg/L]	Pb (II) [100 mg/L]	Cd (II) [100 mg/L]	Pb (II) [100 mg/L]
Pseudo-first-order				
q_e (mg.g^{-1})	~149	~205	~112	~275
k_1 (min)	0.06	0.07	0.06	0.07
R^2	0.97	0.98	0.96	0.98
Pseudo-second-order				
q_e (mg.g^{-1})	~370	~442	~344	~464
k_2 ($\times 10^3$ g.mg^{-1}.min^{-1})	1.02	0.75	0.98	0.86
R^2	0.99	0.99	0.99	0.99
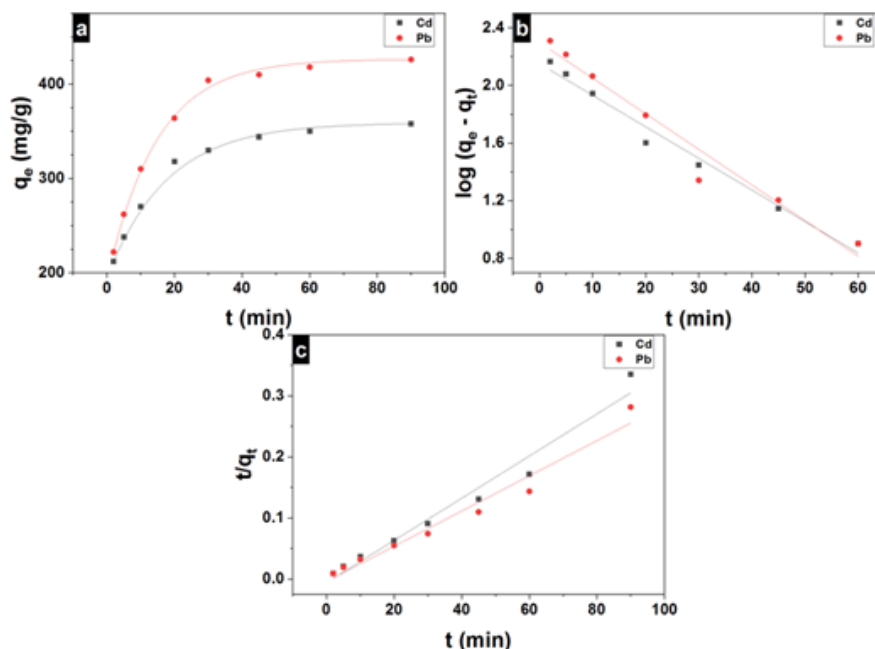
Fig 3. (a) q_e versus t, (b) pseudo-first-order, and (c) pseudo-second-order model plot for Cd (II) and Pb (II) adsorption.

3.3 Adsorption Studies: Binary-component system

The study of multi-component adsorption is important, as a single pollutant is rarely present in industrial wastewater. This type of adsorption is very significant, as it depicts the interference of one pollutant to other. The multi-component adsorption consisting of Cd (II) and Pb (II) were studied and the experimental data was then compared with the data of the single-component system. To better understand the multi-component adsorption, three effects were taken into account. (i) If the interaction between multi-component species when compared is equal to the single-component system ($q_m = q_o$), then the effect is considered to be non-interactive. (ii) If the interaction between multi-component species dominates over a single-component system ($q_m > q_o$), then the effect is considered to be synergistic. (iii) If the effect of a single-component system dominates over the multi-component system ($q_m < q_o$), then the effect is considered to be antagonistic[18,24,25]. Here, the q_m represents the adsorption capacity for a multi-component system and the q_o represents the adsorption capacity for a single-component system.

Hence, adsorption experiments were performed by varying the concentrations of one metal ion and keeping the concentration of other metal ions constant. The maximum adsorption capacity of the nanomaterial at two different initial concentrations, 50 mg/L, and 100 mg/L of Cd (II) keeping the Pb (II) fixed at 0 mg/L, 50 mg/L, and 100 mg/L is presented in Figure 4**a**. Similar experiments were also conducted for (II) and presented in Figure 4**b**. A decrease in adsorption capacity was observed for all concentrations of Cd (II) in the presence of Pb (II) (Figure 4**a**). However, an opposite phenomenon was noticed for Pb (II) adsorption (Figure 4 **b**). $q_m/q_o > 1$ for Pb (II)suggesting the dominance of synergistic effect, and $q_m/q_o < 1$ for Cd (II) suggesting the dominance of antagonistic effect for simultaneous removal of metals ions in a binary system. The possible reasons for easy adsorption of Pb (II) compared to Cd (II) could be the higher values of electronegativity of Pb (II) compared to Cd (II) which may possess a higher electrostatic attraction due to the charge to radius ratio[18,24].

To check the effect of other metal ions on the adsorption capacity of nanomaterial, equilibrium experiments were performed in the presence of both metal ions. The concentrations of the metal ion were varied from 5 to 300 mg/L, and the concentration of Cd (II) and Pb (II) were kept equal to their initial concentrations, i.e., $C_{Cd\,(II)} = C_{Pb\,(II)}$ for all experiments. Estimation of the adsorption capacity was done by measuring the residual ion concentration of the respective samples at equilibrium conditions.

The nature of the q_e versus C_e plot for binary experiments was found to be similar to the single system experimental results (Figure 5**a**) . However, the maximum adsorption capacity was found to be ~475 mg/g for Cd (II) and ~650 mg/g for Pb (II). A reduction in adsorption capacity for Cd (II) and enhancement in adsorption capacity for Pb (II) was observed in binary-
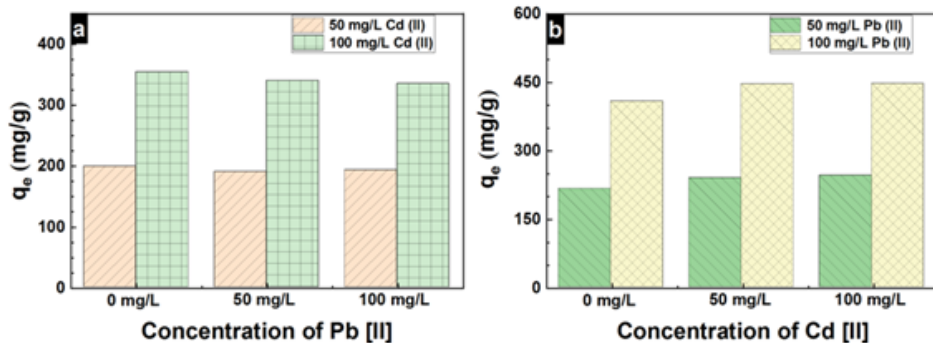
Fig 4. Adsorption capacity of (a) Cd (II) at varied concentration of Pb (II), and (b) Pb (II) at varied concentration of Cd (II) by NiO nanoparticles.

component adsorption compared to single-component adsorption. A comparison chart for the adsorption capacity of Cd (II) and Pb (II) is presented in Table 3. The results indicated that the adsorption capacity in NiO nanoparticles is either comparable or better than the other adsorbents.

The Langmuir and Freundlich isotherm plots are shown in Figure 5b and Figure 5 c, respectively. The constants of the model equations are presented in Table 1. Like single component adsorption studies, in the case of binary adsorption also the Langmuir isotherm was found to be better explaining the experimental results in a better way than the Freundlich isotherm as the R^2 value for Langmuir model fitting is found to be higher than the Freundlich model. Further, computed $R_L < 1$ for both metal ions [R_L = 0.07-0.09 for Cd (II) and 0.04 – 0.8 for Pb (II)] indicating favorable adsorption of ions onto NiO.
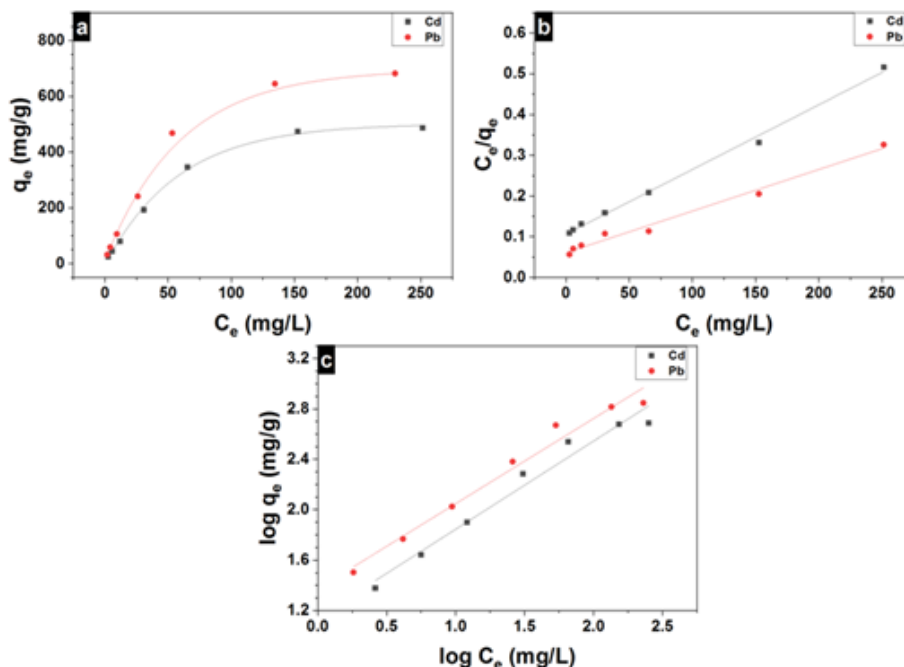
Fig 5. (a) q_e versus Ceplot, (b) Langmuir isotherm, and (c) Freundlich isotherm in a binary-component system.

Table 3. Comparison of adsorption capacity NiO with other adsorbents

Adsorbent	q_{max} (mg.g^{-1})		References
	Cd (II)	Pb (II)	
Dithizone SBA-15	189	208	[26]
Hydroxyapatite/alginate/gelatin NPs	323	575	[25]
Silica Gel	45.5	27.1	[27]
PMMAgMMT	19.27	34.25	[28]
Cystine modified hydrogel	130	263	[29]
Cs-PMA/HNT	303.6	313.7	[30]
NiO	~515	~650	**This work**

A solution of 100 mg/L of Cd (II) and Pb (II) each was used for kinetics studies. The Adsorption capacities of the nanostructure were plotted as a function of time in Figure 6**a.** It is observed that contact of 60 min is enough to achieve the equilibrium, which is similar to the results of the single-component experiments. The kinetic data was further fitted using pseudo-first-order and pseudo-second-order models and presented in Figure 6**b** and Figure 6**c ,** respectively. The values of the constants of the respective model equation are presented in Table 2. A higher magnitude of the R^2 values was observed for pseudo-second-order model fitting compared to the pseudo-first-order model. These observations indicate that the pseudo-second-order model could better explain binary-component adsorption like single-component adsorption.
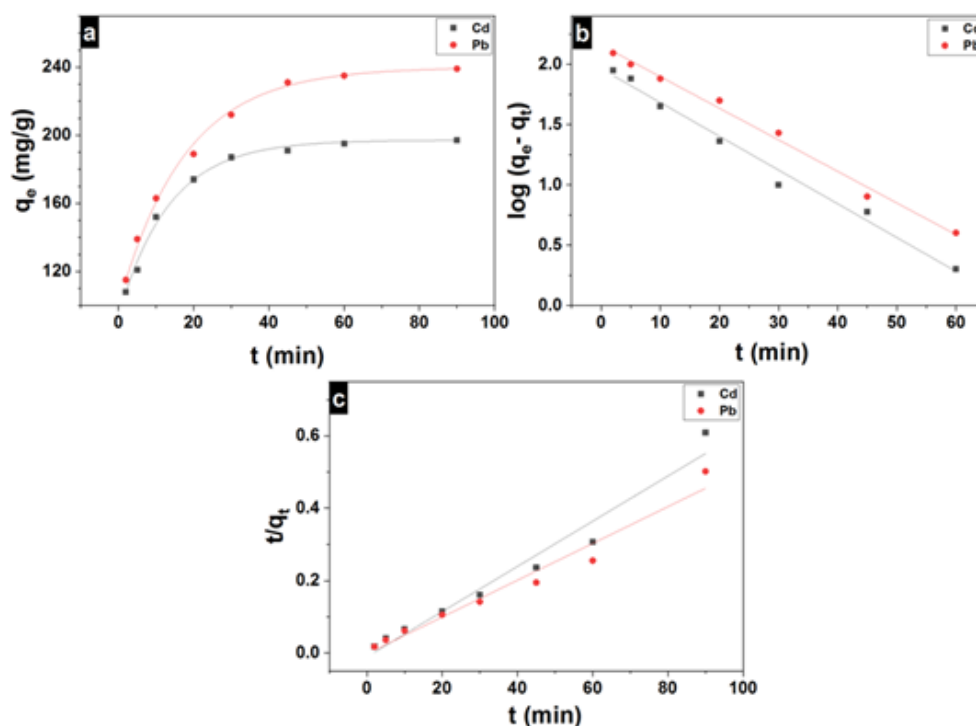
Fig 6. (a) qe versus t plot,(b) Pseudo-first-order and (c) pseudo-second-order model plots.

4 Conclusion

The synthesis of NiO nanostructures through the one-pot synthesis method and the metal ion adsorption studies in one-component and two-component systems have been successfully demonstrated here. The time required to equilibrate the process for simultaneous removal of Cd (II) and Pb (II)from an aqueous solution is found to be 60 min for the one-component and

two-component metal ion removal process. The synthesized NiO showed better adsorption capacity of Cd (II) and PB (II) compared to many reported adsorbents. An increase in adsorption capacity from ~610 mg/g to ~650 mg/g for Pb (II) and a decrease in adsorption capacity from ~515 mg/g to ~475 mg/g for Cd (II) was observed in a two-component system compared to one-component system. These phenomena indicated that the Pb (II), and Cd (II)adsorption is affected by the synergistic and antagonistic effect, respectively. The metal ion adsorption also follows the Langmuir isotherm and pseudo-second-order model in both types of systems. An excellent adsorption capacity and no change in the adsorption mechanism in single- and multiple metal ion-containing solutions make NiO nanoparticles a potential adsorbent for real-life application for metal ions removal from wastewater.

References

1) Wang Y, Li J, Wei Z. Transition-metal-oxide-based catalysts for the oxygen reduction reaction. *Journal of Materials Chemistry A*. 2018;6:8194–8209. Available from: https://doi.org/10.1039/C8TA01321G.

2) Yang T, Song TT, Callsen M, Zhou J, Chai JW, Feng YP, et al. Atomically Thin 2D Transition Metal Oxides: Structural Reconstruction, Interaction with Substrates, and Potential Applications. *Advanced Materials Interfaces*. 2019;6. Available from: https://doi.org/10.1002/admi.201801160.

3) Fang S, Bresser D, Passerini S. Transition Metal Oxide Anodes for Electrochemical Energy Storage in Lithium- and Sodium-Ion Batteries. *Advanced Energy Materials*. 2020;10:1902485. Available from: https://doi.org/10.1002/aenm.201902485.

4) Gohar RS, Ahmad I, Shah A, Majeed S, Najam-Ul-Haq M, Ashiq MN, et al. Fabrication of transition-metal oxide and chalcogenide nanostructures with enhanced electrochemical performances. *Journal of Energy*. 2020;31:101621. Available from: https://doi.org/10.1016/j.est.2020.101621.

5) Lee E, Yoon YS, Kim DJ. Two-Dimensional Transition Metal Dichalcogenides and Metal Oxide Hybrids for Gas Sensing. *ACS Sensors*. 2018;3:2045–2060. Available from: https://doi.org/10.1021/acssensors.8b01077.

6) Joshi N, Hayasaka T, Liu Y, Liu H, N Oliveira O, Lin L. A review on chemiresistive room temperature gas sensors based on metal oxide nanostructures, graphene and 2D transition metal dichalcogenides. *Microchimica Acta*. 2018;185:213. Available from: https://doi.org/10.1007/s00604-018-2750-5.

7) Izzudin NM, Jalil AA, Aziz FFA, Azami MS, Ali MW, Hassan NS, et al. Simultaneous remediation of hexavalent chromium and organic pollutants in wastewater using period 4 transition metal oxide-based photocatalysts: a review. *Environmental Chemistry Letters*. 2021. Available from: https://doi.org/10.1007/s10311-021-01272-1.

8) Gan X, Lei D, Ye R, Zhao H, Wong KY, Kwok-Yin. Transition metal dichalcogenide-based mixed-dimensional heterostructures for visible-light-driven photocatalysis: Dimensionality and interface engineering. *Nano Research*. 2003;14:2003–2022. Available from: https://doi.org/10.1007/s12274-020-2955-x.

9) Yousefi SR, Ghanbari D, Masoud SN, Hassanpour M. Photo-degradation of organic dyes: simple chemical synthesis of Ni(OH)2 nanoparticles, Ni/Ni(OH)2 and Ni/NiO magnetic nanocomposites. *Journal of Materials Science: Materials in Electronics*. 2016;27:1244–1253. Available from: https://doi.org/10.1007/s10854-015-3882-6.

10) Liu G, Abukhadra, Mostafa R, El-Sherbeeny AM, Mostafa AM, Elmeligy MA. Insight into the photocatalytic properties of diatomite@Ni/NiO composite for effective photo-degradation of malachite green dye and photo-reduction of Cr (VI) under visible light. *Journal of Environmental Management*. 2020;254:109799. Available from: https://doi.org/10.1016/j.jenvman.2019.109799.

11) Sharma A, Kositski R, Kovalenko O, Mordehai D, Rabkin E. Giant shape- and size-dependent compressive strength of molybdenum nano- and microparticles. *Acta Materialia*. 2020;198:72–84. Available from: https://doi.org/10.1016/j.actamat.2020.07.054.

12) Christiansen TL, Cooper SR, M Ø Jensen K. There's no place like real-space: elucidating size-dependent atomic structure of nanomaterials using pair distribution function analysis. *Nanoscale*;2020:2234–2254. Available from: https://doi.org/10.1039/D0NA00120A.

13) Raha S, Ahmaruzzaman M. Enhanced performance of a novel superparamagnetic g-C3N4/NiO/ZnO/Fe3O4 nanohybrid photocatalyst for removal of esomeprazole: Effects of reaction parameters, co-existing substances and water matrices. *Chemical Engineering Journal*. 2020;395:124969. Available from: https://doi.org/10.1016/j.cej.2020.124969.

14) Akbari A, Sabouri Z, Hosseini HA, Hashemzadeh A, Khatami M, Darroudi M. Effect of nickel oxide nanoparticles as a photocatalyst in dyes degradation and evaluation of effective parameters in their removal from aqueous environments. *Inorganic Chemistry Communications*. 2020;115:107867. Available from: https://doi.org/10.1016/j.inoche.2020.107867.

15) Gopi S, M Al-Mohaimeed A, Elshikh MS, Yun K. Facile fabrication of bifunctional SnO-NiO heteromixture for efficient electrocatalytic urea and water oxidation in urea-rich waste water. *Environmental Research*. 2021;201:111589. Available from: https://doi.org/10.1016/j.envres.2021.111589.

16) Wang Z, Shen Q, Xue J, Jia H, Xu B, Liu X, et al. Annealing temperature effect on 3D hierarchically porous NiO/Ni for removal of trace hexavalent chromium. *Materials Chemistry and Physics*. 2020;240:122140. Available from: https://doi.org/10.1016/j.matchemphys.2019.122140.

17) Shivangi, Bhardwaj S, Sarkar T. Core-shell type magnetic Ni/NiO nanoparticles as recyclable adsorbent for Pb (II) and Cd (II) ions: One-pot synthesis, adsorption performance, and mechanism. *Journal of the Taiwan Institute of Chemical Engineers*. 2020;113:223–230. Available from: https://doi.org/10.1016/j.jtice.2020.08.011.

18) Shivangi, Bhardwaj S, Sarkar T. Simultaneous removal of cadmium and lead ions from aqueous solutions by nickel oxide-decorated reduced graphene oxides. *International Journal of Environmental Science and Technology*. 2021. Available from: https://doi.org/10.1007/s13762-021-03510-z.

19) Xiang W, Zhang X, Chen J, Zou W, He F, Hu X, et al. Biochar technology in wastewater treatment: A critical review. *Chemosphere*. 2020;252:126539. Available from: https://doi.org/10.1016/j.chemosphere.2020.126539.

20) Chai WS, Cheun JY, Kumar PS, Mubashir M, Majeed Z, Banat F, et al. A review on conventional and novel materials towards heavy metal adsorption in wastewater treatment application. *Journal of Cleaner Production*. 2021;296:126589. Available from: https://doi.org/10.1016/j.jclepro.2021.126589.

21) Fu F, Wang Q. Removal of heavy metal ions from wastewaters: A review. *Journal of Environmental Management*. 2011;92:407–418. Available from: https://doi.org/10.1016/j.jenvman.2010.11.011.

22) Mahmoud AED, M Al-Qahtani K, O Alflaij S, F Al-Qahtani S, A Alsamhan F, et al. Green copper oxide nanoparticles for lead, nickel, and cadmium removal from contaminated water. *Scientific Reports*. 2021;11:12547. Available from: https://doi.org/10.1038/s41598-021-91093-7.

23) Nakate UT, Ahmad, Rafiq, Patil, Yu YT, Hahn YB. Ultra thin NiO nanosheets for high performance hydrogen gas sensor device. *Applied Surface Science*. 2020;506.

24) Roy A, Bhattacharya J. A binary and ternary adsorption study of wastewater Cd(II), Ni(II) and Co(II) by γ-Fe2O3 nanotubes. *Separation and Purification Technology*. 2013;115:172–179. Available from: hhttps://doi.org/10.1016/j.seppur.2013.05.010.

25) Sangeetha K, Vidhya G, Vasugi G, Girija EK. Lead and cadmium removal from single and binary metal ion solution by novel hydroxyapatite/alginate/gelatin nanocomposites. *Journal of Environmental Chemical Engineering*. 2018;6:1118–1126. Available from: https://doi.org/10.1016/j.jece.2018.01.018.

26) Behbahani M, Salarian M, M Amini M, Sadeghi O, Bagheri A, Bagheri S. Application of a New Functionalized Nanoporous Silica for Simultaneous Trace Separation and Determination of Cd(II). *Food Analytical Methods*. 2013;6:1320–1329. Available from: https://doi.org/10.1007/s12161-012-9545-9.

27) Xu H, Wu Y, Wang J, Shang X, Jiang X. Simultaneous preconcentration of cadmium and lead in water samples with silica gel and determination by flame atomic absorption spectrometry. *Journal of Environmental Sciences*. 2013;25:45–49. Available from: https://doi.org/10.1016/S1001-0742(14)60624-0.

28) Bunhu T, Tichagwa L, Chaukura N. Competitive sorption of Cd2+ and Pb2+ from a binary aqueous solution by poly (methyl methacrylate)-grafted montmorillonite clay nanocomposite. *Applied Water Science* . 2017;7:2287–2295. Available from: https://doi.org/10.1007/s13201-016-0404-5.

29) Karbarz M, M Khalil A, Wolowicz K, Kaniewska K, Romanski J, Stojek Z. Efficient removal of cadmium and lead ions from water by hydrogels modified with cystine. *Journal of Environmental Chemical Engineering*. 2018;6:3962–3970. Available from: https://doi.org/10.1016/j.jece.2018.05.054.

30) Maity J, Ray SK. Chitosan based nano composite adsorbent-Synthesis, characterization and application for adsorption of binary mixtures of Pb(II) and Cd(II) from water. *Carbohydrate Polymers*. 2018;182:159–171. Available from: https://doi.org/10.1016/j.carbpol.2017.10.086.